



HAL
open science

Operando kinetics of hydrogen evolution and elemental dissolution I: The dissolution of galvanized steel in hydrochloric acid

Baojie Dou, Xuejie Li, Junsoo Han, Kevin Ogle

► **To cite this version:**

Baojie Dou, Xuejie Li, Junsoo Han, Kevin Ogle. Operando kinetics of hydrogen evolution and elemental dissolution I: The dissolution of galvanized steel in hydrochloric acid. *Corrosion Science*, 2023, 214, pp.111007. 10.1016/j.corsci.2023.111007. hal-03969836

HAL Id: hal-03969836

<https://cnrs.hal.science/hal-03969836>

Submitted on 2 Feb 2023

HAL is a multi-disciplinary open access archive for the deposit and dissemination of scientific research documents, whether they are published or not. The documents may come from teaching and research institutions in France or abroad, or from public or private research centers.

L'archive ouverte pluridisciplinaire **HAL**, est destinée au dépôt et à la diffusion de documents scientifiques de niveau recherche, publiés ou non, émanant des établissements d'enseignement et de recherche français ou étrangers, des laboratoires publics ou privés.

***Operando* kinetics of hydrogen evolution and elemental dissolution I:**

The dissolution of galvanized steel in hydrochloric acid

Baojie Dou^{a,b,c}, Xuejie Li^{a,d}, Junsoo Han^c, Kevin Ogle^{a*}

a) Chimie ParisTech, PSL University, CNRS, Institut de Recherche Chimie ParisTech (IRCP), F-75005, Paris, France

b) School of Materials Science and Engineering, Sichuan University of Science & Engineering, 643000, Zigong, China

c) Sorbonne Université, Laboratoire Interfaces et Systèmes Electrochimiques, LISE, F-75005, Paris, France

d) Department of Chemistry, Western University, London, ON, N6A 5B7, Canada

*Corresponding author. E-mail: kevin.ogle@chimieparistech.psl.eu (Kevin Ogle)

Keywords: galvanized steels, acid corrosion, hydrogen evolution, operando spectroscopy, intermetallics, kinetics

Abstract

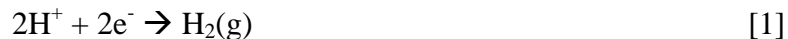
A new approach to the simultaneous measurement of the hydrogen evolution reaction (HER) and elemental dissolution rates is presented and applied to the reaction of galvanized steel coatings with HCl solution. Dissolution profiles revealed several kinetic regimes including the dissolution of the intact coating, the dissolution of the nanometric Fe₂Al₅ intermetallic layer, and the corrosion of the steel substrate. The HER and Zn dissolution rates were in excellent agreement, and the quantities of interfacial Fe and Al were consistent with the predicted 50 nm thick Fe₂Al₅ intermetallic film, demonstrating the analytical capabilities of the atomic emission spectroelectrochemistry (AESEC) technique.

1. Introduction

The formation of hydrogen gas is a common by-product of many corrosion processes, and the volumetric measurement of hydrogen is a well-accepted method of monitoring the rate of corrosion. The standard methodology uses a burette or other glass receptacle to directly measure the volume of hydrogen produced [1-5]. Interestingly, similar methodologies date to the early years of chemical history when experimenters were isolating individual gases and working out the stoichiometry of basic chemical reactions [6]. More recently, the gravimetric methodology underwent extensive development by the work of Curioni [7,8] and Frankel [9] who transformed the volumetric measurement into a gravimetric method *via* the principle of Archimedes. This methodology has been applied to the anomalous hydrogen formation during the corrosion of Al [10] and the evolution of oxygen during the anodization of Al alloy [11]. This work has inspired development of respirometry techniques conducted by Strebl *et al.* [12] with atmospheric corrosion applications.

These methods permit the measurement of gas during an electrochemical experiment and the correlation of the hydrogen gas evolution rate with the electrical current. However, for most corrosion reactions, elemental dissolution and oxide formation occur simultaneously with gas formation and electron transfer. To perform a complete mass-charge balance, independent measurements of at least three of these coupled phenomena are necessary. The coupling of real-time volumetric techniques with element-resolved electrochemistry was first attempted by Lebouil *et al.* [13,14] using a video recorder and a specialized image analysis software to calculate bubble size as they passed through a micro-fluidic cell in transit to a downstream inductively coupled atomic emission spectrometer (ICP-AES) for elemental analysis. The methodology was simplified by Han *et al.* [15] who combined the Curioni's balance method with the atomic emission spectroelectrochemistry (AESEC) flow cell. This was used to demonstrate a complete mass-balance during the cathodic corrosion of an aluminum alloy.

The standard method of validating the volumetric measurement of hydrogen evolution is by comparing the measured rate of the HER with an applied cathodic current where the dominant cathodic reaction is hydrogen formation (Eq. [1]). This will validate the relationship between faradaic charge transfer and volumetric hydrogen but does not consider the relationship with metal dissolution.



For the latter, the dissolution of a galvanized steel in acid solution represents an ideal validation method as it represents a well-defined quantity of Zn with a well-known dissolution stoichiometry in acid solution:



Therefore, the rates of Zn^{2+} formation (ICP-AES) and $\text{H}_2(\text{g})$ evolution (balance) should be in a 1:1 stoichiometry independent of the dissolution conditions. As the dissolution rate may be readily varied by changing the acidity of the electrolyte, the direct measurement of Zn dissolution and hydrogen formation rates may be compared over a wide range of different kinetic conditions.

The use of a galvanized steel coating as a reference material also demonstrates the sensitivity of the AESEC technique to nanometric films. During the galvanization process with a molten 0.1 - 1 at.% Al-Zn bath, an intermetallic film is formed between the zinc coating and the steel substrate, presumably in the form of $\text{Fe}_2\text{Al}_5\text{Zn}_x$ ($0 < x < 1$) [16-20]. This film, on the order of 20 - 50 nm, inhibits the formation of Fe-Zn intermetallic phase or “outbursts” that are detrimental to the mechanical properties of the final coating. The AESEC technique was originally developed to quantify this interfacial intermetallic layer although this application has never been published except for a typical result given in the original patent of the AESEC method [21].

In this work we present an amelioration of the previous method of hydrogen analysis, discuss its ability to monitor transient events, and demonstrate its use applied to the dissolution of a galvanized steel coating. In this way, the total quantity of Zn and its stoichiometric relationship to hydrogen during a transient dissolution have been evaluated and the analytical sensitivity of the method to nanometric films is demonstrated. Further, different kinetic regimes of the dissolution reaction are clearly distinguished allowing for a more refined interpretation of the conventional open circuit potential vs. time curve. This type of analysis is important for a deeper understanding of the different reaction steps during spontaneous open circuit reactions such as surface pickling and conversion coating treatments.

2. Experimental

2.1. Instrumentation

The ICP-AES system (Horiba Ultimat 2CTM) was equipped with a polychromator with an array of photon detectors for simultaneous measurement of up to 30 elements, and a monochromator for a higher resolution measurement of a single element. Both were nitrogen purged. Emission intensities at 213.86, 167.08, and 259.94 nm were used to determine the Zn, Al and Fe concentrations respectively. Al was measured from the monochromator, and Zn and Fe from the polychromator. Mass measurements were performed with a Mettler Toledo ME204TM balance with ± 0.1 mg sensitivity and with a time resolution of 1 point per second. A Gamry Reference 600TM potentiostat and galvanostat was used to perform the electrochemical experiments. The three-electrode electrochemical flow cell used for AESEC has been previously described [22]. A saturated calomel electrode (SCE) as a reference electrode and a Pt foil as a counter electrode were used in all experiments. A Pt foil was used as a working electrode for hydrogen evolution reaction (HER) under different cathodic currents.

2.2. Materials

A commercial hot-dip galvanized steel (HDG) with an average coating thickness of 20 μm according to the supplier was used in this work. The galvanized steel was used as received following an ethanol rinse. Deionized water of 18.2 M Ω cm produced with a Millipore Milli-QTM system and reagent grade NaCl and HCl were used to prepare the electrolytes.

2.3. Gas collection and measurement

A schematic diagram of the apparatus is shown in Fig. 1. The flow rate through the cell was controlled at approximately 3 mL min⁻¹ by peristaltic pump 1, $f(p1)$. Immediately after the flow cell, the electrolyte was split *via* a specially designed, 3D printed T-junction. The flow to the ICP-AES was controlled at approximately 1 mL min⁻¹ by peristaltic pump 2, $f(p2)$. The remainder of the electrolyte and the hydrogen bubbles continued freely up to the hydrogen collection beaker at a rate of approximately 2 mL min⁻¹, ($= f(p1) - f(p2)$). The T-junction was specially designed to ensure that the hydrogen bubbles would be carried preferentially along the vertical path to the hydrogen collection beaker rather than be diverted to the ICP-AES, as

demonstrated in section 3.1. The flow rate through the cell was carefully measured to a precision of $> \pm 1$ % for each series of experiments.

The hydrogen bubble collection cell was set up with either the electrolyte of the experiment or a NaCl solution chosen to match the density of the electrolyte. (The substitution was performed to avoid security risk of using a large, suspended volume of acid.) The beaker contained a few milliliters of air such that the hydrogen partial pressure would remain negligibly small to limit the redissolution of hydrogen once it had arrived in the collection beaker. The temperature of the laboratory room was not controlled but varied around 23 ± 2 °C. The galvanostatic experiments were performed with ice in the collection bath to maintain a constant temperature of approximately 7 °C. Some experiments were performed using a hydrogen generator to pre-saturate the electrolyte before it reached the flow cell. However, these experiments did not show a significant improvement and were not reproducible. The results presented here therefore were performed without the hydrogen generator.

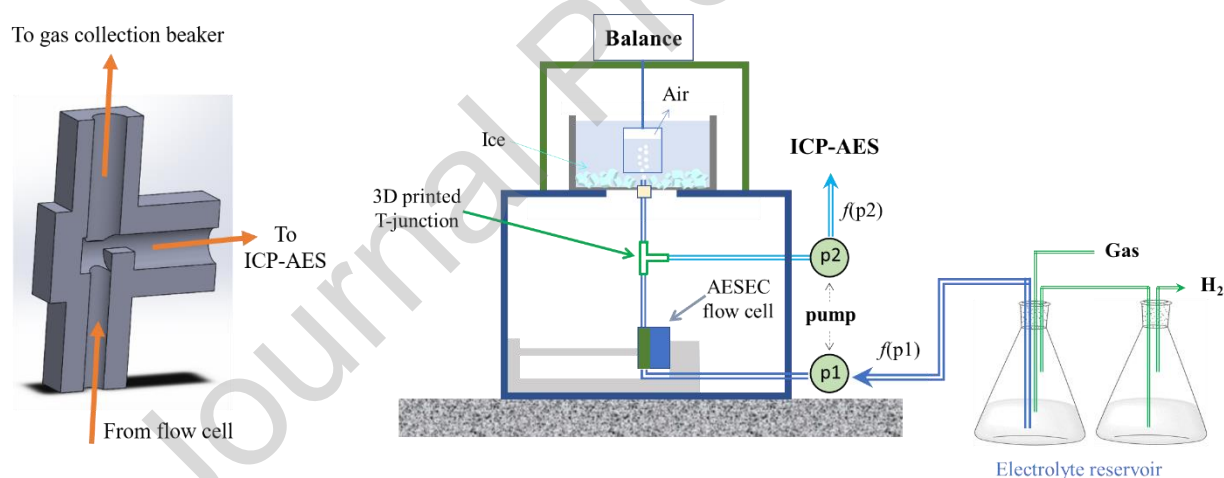


Fig. 1. Schematic of the experimental set-up. The 3D printed T-junction is shown to the left.

2.4 Calculations

The dissolution rate of the element (v_M , in mol s^{-1}) was determined from the elemental concentration (C_M) measured by the AESEC technique:

$$v_M = f(p1) C_M \quad [3]$$

where $f(p1)$ is the flow rate of the electrolyte through the cell (first pump, p1). For convenience, the dissolution rate may be presented as an equivalent faradaic current (i_M) using Faraday's law:

$$i_M = n_M F v_M \quad [4]$$

where n_M is the number of electrons exchanged in the dissolution reaction and F is the Faraday constant.

The volume of hydrogen produced, ΔV_{H_2} , was calculated from the mass change ($\Delta mass$) recorded by the balance using Archimedes' principle and the density of the electrolyte, ρ_{el} (Eq. [5]). This was in turn converted into moles of hydrogen produced, $Q(H_2)$,¹ by the ideal gas equation:

$$\Delta V_{H_2} = \Delta mass / \rho_{el} \quad [5]$$

$$Q(H_2) = P \Delta V_{H_2} / RT \quad [6]$$

where R is the ideal gas constant (8.3145 J K^{-1}) and T is temperature in Kelvin. The height of the electrolyte above the collection beaker, approximately 1 – 2 cm (corresponding to a few mL), was ignored in the calculation. The atmospheric pressure (P) given for Paris on the day of the experiment [23] was assumed, typically 1021 hPa (1.01 atm).

The rate of the hydrogen evolution reaction, v (HER), from Eq. [1] was estimated from a numerical derivative of $Q(H_2)$,

$$\delta Q(H_2)_j = (Q(H_2)_{j+1} - Q(H_2)_j) / \Delta t \quad [7]$$

where Δt is the time between data points with $\Delta t = 1 \text{ s}$ in all experiments described herein. The data consisted of discrete jumps of mass due to the sequential arrival of bubbles into the collection beaker and therefore the value of $\delta Q(H_2)$ does not reflect the instantaneous HER rate. Therefore, a moving average smoothing routine was used to determine hydrogen evolution rate considered instantaneous over the time scale as:

¹ In this work, the symbol n is used for the number of electrons transferred in an electrochemical reaction, therefore Q , is used for the number of moles of H_2 in keeping with the conventional terminology of AESEC.

$$v(\text{HER})_j = \sum_{j-k}^{j+k} \delta Q(\text{H}_2)_j / (2k+1) \quad [8]$$

To facilitate comparison with the simultaneously measured electrical current, the $v(\text{HER})$ may be expressed as an electrical current by Faraday's law, analogous to Eq. 4 :

$$i_{\text{H}_2} = n F v(\text{HER}) \quad [9]$$

where $n = 2$ is the number of electrons in Eq. [1] and F is the Faraday constant.

3. Results and discussion

3.1. Electrochemical Stoichiometry

Typical profiles showing the evolution of hydrogen gas as a function of time cathodic are shown in Fig. 2. The measured ΔV_{H_2} transients converted to $Q(\text{H}_2)$ using Eq. [6] (red and blue curves) are compared with the expected $Q(\text{H}_2)$ (gray lines) for each applied cathodic current, assuming Faraday's law with a 100% faradaic efficiency. Experiments were performed with the pump of the ICP-AES on (red lines) or without (blue lines) to verify that the hydrogen bubbles were efficiently transferred to the collection chamber. No significant difference in the rates was observed.

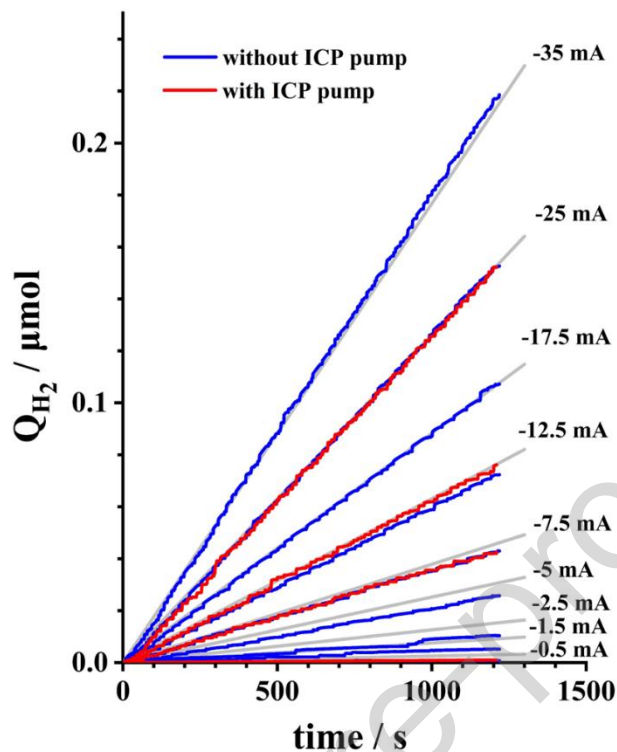


Fig. 2. Quantity of H_2 determined from the recorded mass change (Eqs. [5] and [6]) as a function of time for different applied cathodic currents for Pt in 1.0 M NaCl, pH = 6.4 as indicated. The gray lines represent the expected values for the applied current assuming Faraday's law with 100% cathodic efficiency. The electrode surface area was 0.5 cm^2 . Red and blue curves were recorded with and without the ICP-AES pump (p2 in Fig. 1).

The average hydrogen evolution rate (i_{H_2}) was calculated by Eqs. [5 – 7] and is shown as a function of the applied cathodic current ($-i_e$) in Fig. 3. This curve also includes data measured at constant potential (potentiostatic). For the potentiostatic measurements, constant potentials of -2.8 V, -2.2 V, -1.9 V, -1.5 V and -1.1 V vs. SCE were applied for 1200 s (See also Appendix I.2(d)). In this case, the gravimetric measurement is compared with the average current value.

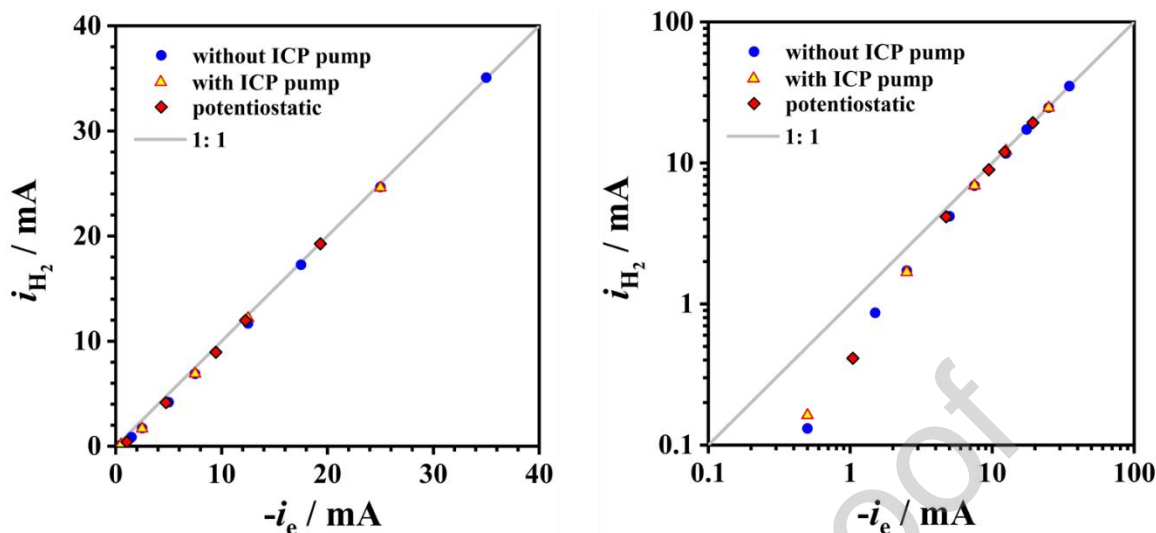


Fig. 3. Quantity of H_2 as a function of the applied cathodic current ($-i_e$). The electrode surface area was 0.5 cm^2 . The red diamonds are the results of potentiostatic experiments in which the HER rate is plotted versus the average of the cathodic current density ($-i_e$) transient. The log-log plot (right) is shown to better illustrate the difference in the low current range, $-i_e < 5 \text{ mA}$. The solid line indicates the hypothetical 1:1 relationship. The original profiles are available in *Annexe I.2*.

For $-i_e > 5 \text{ mA}$, the data shows a good agreement between the measured equivalent hydrogen evolution rate and applied (or average) cathodic current. For $-i_e < 5 \text{ mA}$ the measured hydrogen current is systematically below the applied or average current for the potentiostatic experiments. The lower-than-expected current is probably due to the formation of dissolved hydrogen predominating over bubble formation. The excellent agreement between the results with and without the ICP-AES pump over the entire current range demonstrates that, essentially all the hydrogen goes to the gas collection system and is not siphoned off to the aspiration system of the plasma during the operating conditions of these experiments. Likewise, no obvious distinction may be made between the potentiostatic and galvanostatic experiments.

3.2. Dissolution Stoichiometry

The stoichiometry between hydrogen evolution and the elemental dissolution rate transients in the absence of electrochemical control was investigated by dissolving a galvanized steel coating in HCl solutions. The coating consists of a continuous hot-dip Zn-Al alloy (approximately 0.2 wt.% Al) with a nominal thickness of $20 \mu\text{m}$ as provided by the supplier. During the galvanizing process, the Al reacts with the Fe to form a thin film of Fe-Al

intermetallic phase, with a known Fe / Al stoichiometry of Fe_2Al_5 . During the dissolution of the coating in HCl solution, the different layers react sequentially – first the Zn coating, second the interfacial film, and finally the underlying steel substrate.

Fig. 4 gives the dissolution profiles for the galvanized steel in different HCl concentrations. Shown as a function of time are the dissolution rates of Zn, Al and Fe as measured by AESEC, the hydrogen evolution rate as measured by the gravimetric system using the balance, and the open circuit potential monitored simultaneously by the potentiostat. Note that the Al and Fe dissolution rates have been multiplied by 40 and 100 respectively to be on the same scale as the Zn dissolution and HER rates. The 40/100 ratio was chosen to respect the stoichiometry of the interfacial Fe_2Al_5 intermetallic. For $t < 0$, the electrolyte bypassed the flow cell to determine the emission signal at the background level.

Table 1. Integration of each alloying elements and corrected H_2 in μmol from Fig. 4. Al and Fe were calculated from the third domain (III) to investigate the stoichiometry of the intermetallic phase.

HCl / M	H_2 / μmol	Zn / μmol	Al (zone III) / μmol	Fe (zone III) / μmol	Zn/ H_2	Thickness (Zn) / μm	Interface Al/Fe (zone III)
0.5	205	186	0.60	0.25	0.91	18.8	2.4
1.0	235	220	0.82	0.38	0.94	21.5	2.2
2.0	218	220	0.81	0.32	1.01	20.0	2.5
4.0	209	201	0.85	0.32	0.96	19.2	2.6
Average	217	207	0.77	0.32	0.95	19.9	2.4
Standard deviation	10	13	0.09	0.03	0.03	0.9	0.1

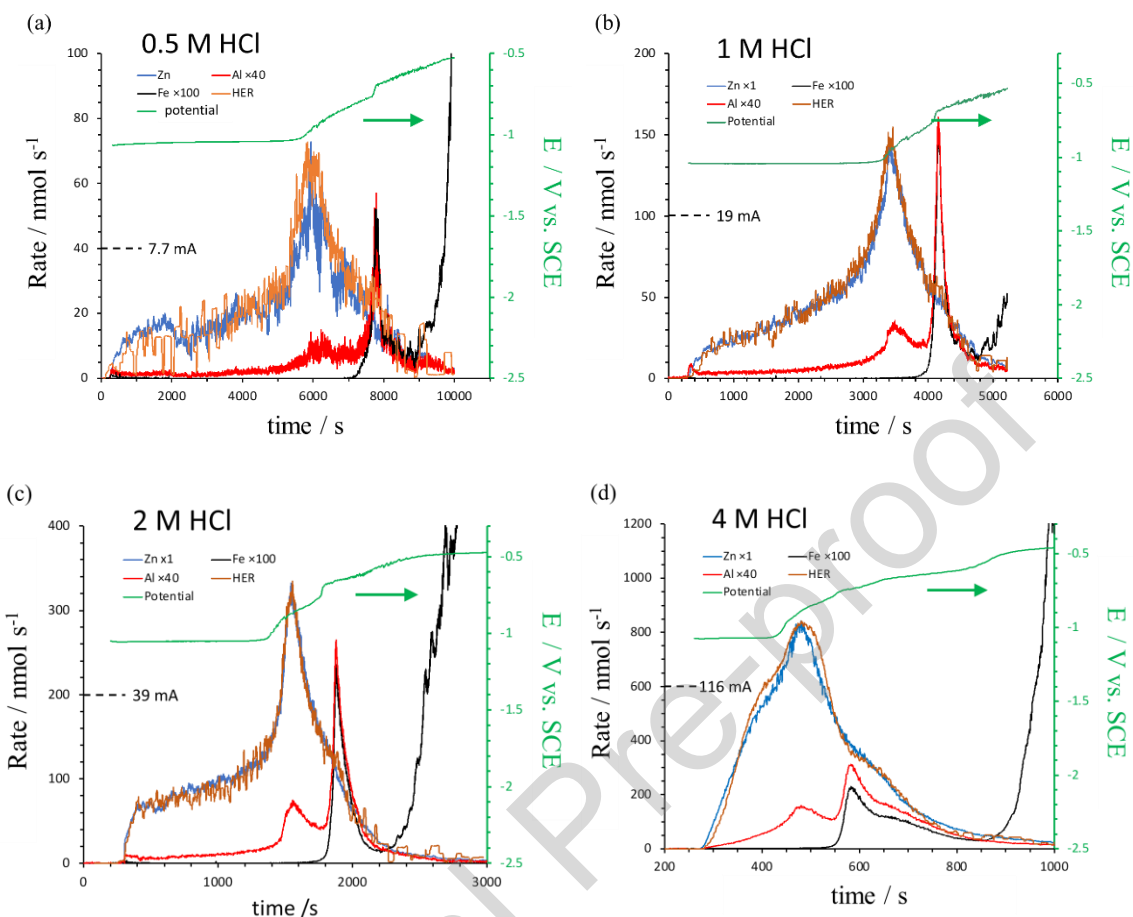


Fig. 4. Open circuit dissolution profiles of a Zn-Al galvanized steel coating in HCl with different concentrations showing Zn, Al, and Fe elemental dissolution rates, HER rates, and the open circuit potential (E) as a function of time. The surface area was 1.0 cm^2 . The current values provided on the y-axis indicate equivalent currents corresponding the elemental dissolution rates for comparison with Fig. 3.

The sequential attack is demonstrated by the dissolution profiles in Fig. 4. Four different kinetic domains may be identified regardless of the HCl concentration, each corresponding to a different open circuit potential range. The first domain (I) occurs with a potential of -1.1 V vs. SCE and corresponds to the first steps of the Zn coating dissolution. In the second domain (II), the Zn dissolution rate rises abruptly and reaches a maximum while the potential shifts to approximately -0.76 V vs. SCE . This most likely corresponds to a period when the intermetallic film and steel substrate is firstly exposed to the electrolyte, thereby accelerating Zn dissolution *via* bimetallic coupling. Throughout the first and second kinetic domains, Al dissolution is also observed. The third domain (III) is marked by sharp peaks in the Fe and Al dissolution rates which, on the normalized scale shown here, appear to be nearly equal indicative of the 2 to 5

stoichiometric ratio of the intermetallic Fe_2Al_5 layer. The potential shifts to approximately -0.65 V vs. SCE in this domain. Finally in the fourth domain (IV), the Al and Fe dissolution rates decrease and then Fe dissolution rate increases rapidly with a potential shift to approximately -0.48 V vs. SCE. This corresponds to the dissolution of the steel after removal of the Zn coating and the interfacial intermetallic film.

To aid in the stoichiometric analysis, Fig. 5 gives the integrated profiles of Fig. 4. Shown are the dissolved elements in moles (Q_{Zn} , Q_{Al} , and Q_{Fe}) calculated from Eq. [3] and hydrogen (Q_{H_2}) calculated from Eq. [6] as a function of time. Table 1 provides the quantity of each alloying element and collected H_2 from Fig. 4. Note that Al and Fe are given from the third domain (III) in order to calculate the ratio between Al and Fe, giving the composition of the Fe-Al intermetallic phase.

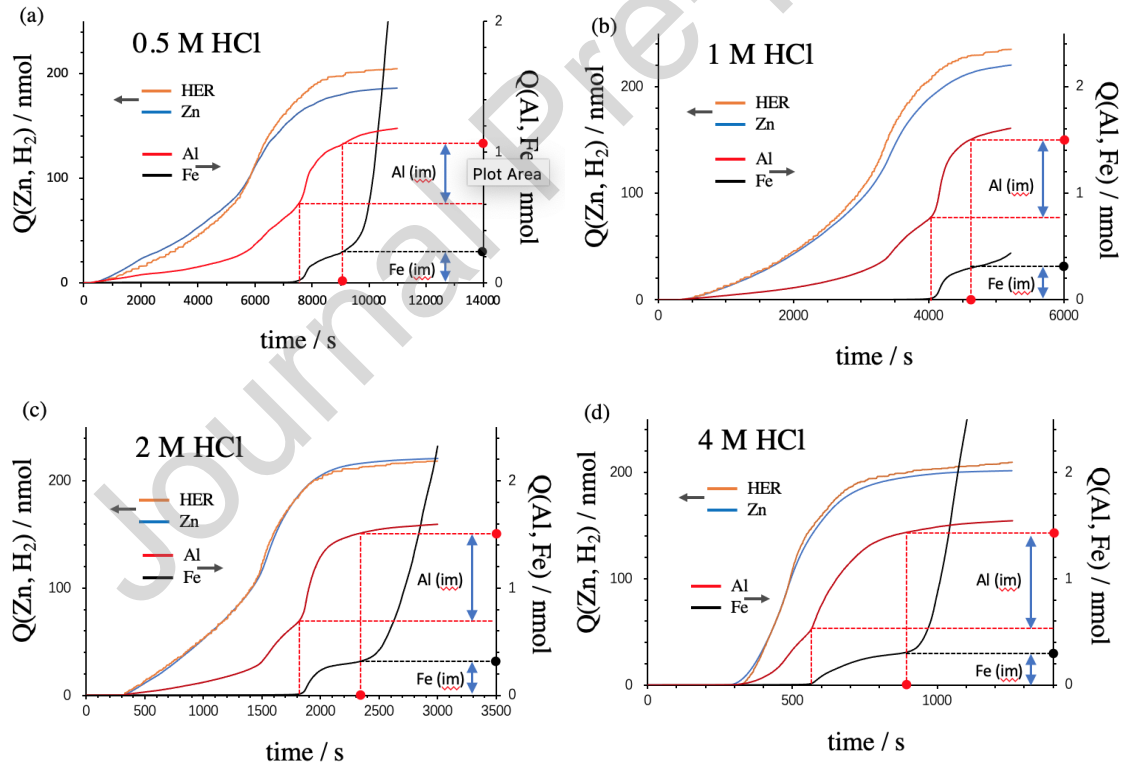


Fig. 5. Quantity of each alloying element and HER integrated from dissolution profiles of Fig. 4. The dashed lines show the method of determining the quantity of Al and Fe in the interfacial Al-Fe alloy (zone III).

A good correlation between the Zn dissolution rate and the HER rate was observed throughout the profiles in Figs. 4 and 5 with an average stoichiometry of $\text{Zn}/\text{H}_2(\text{g})$ of 0.95 ± 0.04 , as shown in the second y-axis in Fig. 6. The integral of the Zn dissolution rate transient from Fig. 5 in average was $207 \pm 16 \mu\text{mol}$ corresponding to an estimated coating thickness of $19.9 \pm 0.9 \mu\text{m}$ (Fig. 6 and Table 1, density of Zn: 7.13 g cm^{-3}), in excellent agreement with the announced nominal thickness of $20 \mu\text{m}$ from the supplier.

The dissolution profiles in the third domain (III) permit the quantification of the interfacial layer (Table 1) which is difficult to access by other methods. The average Al/Fe ratio was determined as 2.4 ± 0.1 again in good agreement with the predicted stoichiometry of the Fe_2Al_5 intermetallic phase. Based on the integral of the Fe dissolution peak in Fig. 5 ($0.32 \pm 0.03 \mu\text{mol Fe}$, see Table 1) and the estimated density of the Fe_2Al_5 intermetallic phase of 7.9 g cm^{-3} [24], a total thickness of $50 \pm 8 \text{ nm}$ of the Fe_2Al_5 intermetallic layer was determined, consistent with transmission electron microscopic analysis for this class of coating materials [20]. This demonstrates the capability to detect the dissolution of nanometer level thin films by AESEC.

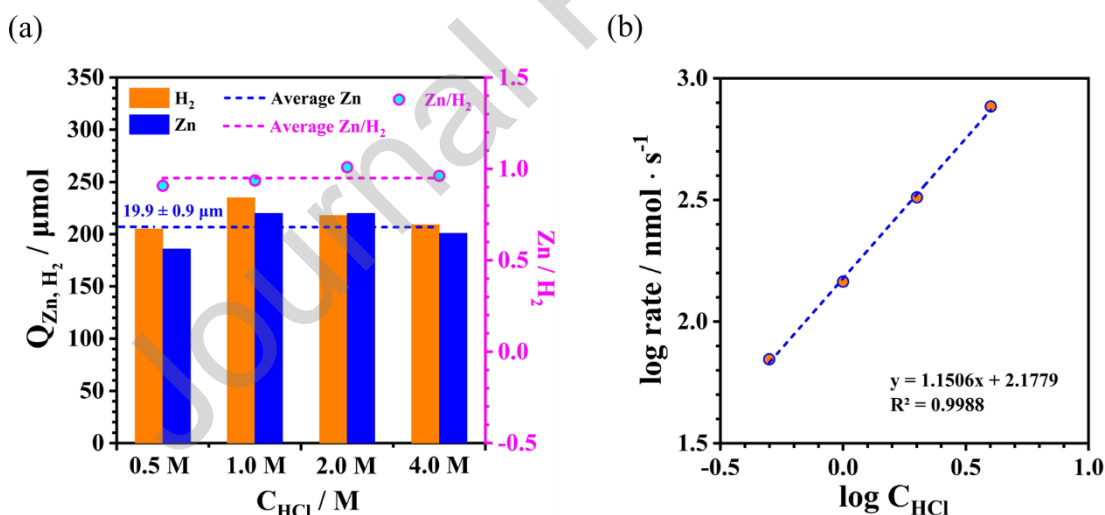


Fig. 6. (a) Quantitative analysis of Zn and H_2 as a function of HCl concentration revealing an estimated coating thickness of a $20 \pm 1 \mu\text{m}$ Zn-Al galvanized coating. (b) The maximum dissolution rate of Zn (or the HER rate assuming they are 1:1) vs. HCl concentration (from Fig. 4), revealing a first order reaction rate dependence.

The elemental dissolution rates in all domains increase with increasing HCl concentration as shown in Fig. 6b. In 4 M HCl, the first and second domains are not clearly distinguished (Figs.

4 and 5). The Zn dissolution rate (or HER rate) maximum increases with first order kinetics (slope = 1.15, $R^2 = 0.999$) as shown in Fig. 6(b).

3.3. Bubble transient analysis

The nature of the hydrogen evolution data differs from that of the electrochemical and spectroscopic measurements, thus the comparison of the different data sets requires some care. Each individual bubble arriving in the collection cell gives rise to a step in the mass measurement. This is seen in the gravimetric mass transients of Fig. 2 which show a staircase progression as bubbles arrive in the collection cell as unique events. The bubbles grow on the Pt surface for a period, then detach and move towards the collection cell. Fig. 7 compares the raw derivative data (δQ_{H_2} in Eq. [7]) and the smoothed version for the four HCl concentrations from Fig. 4. Inspection of the data indicates that the bubble size changes very little as the HER rate varies; rather it is the time between events that decreases. This situation requires the use of a smoothing routine to extract the HER rate as a function of time from the data. Obviously, the degree of smoothing necessary will depend on the HER rate. The data is therefore similar to the detection of second phase particles released during the corrosion / etching of Al alloys [25]. The smoothing routine may be considered as a form of convolution such as is routinely applied in AESEC experiments to compare electrochemical currents with dissolution data. This is necessary since electrochemical currents are essentially instantaneous on the time scale of these experiments, while concentration transients are broadened due to the residence time distribution of the flow cell and diffusional broadening in the capillaries [26, 27]. The development of a similar convolution model for the gravimetric hydrogen is possible, but will require an in depth analysis of the gravimetric hydrogen response function and is beyond the scope of this work.

The use of the simple moving average smoothing routine described here (Eqs. [7] and [8]) may be adjusted by varying the value of k . This is shown in Fig. 8 for the reaction at 4 M HCl where the dissolution and HER rates are extremely intense. In this situation, the arrival of H_2 to the collection cell is so rapid that only a modest smoothing is necessary. For the $k = 5$ dataset in Fig. 8(b), the HER rate shows a higher time resolution than the Zn concentration transient. At $k = 40$, the value used in Fig. 8(c), the two data sets resemble each other closely. The smoothing has no effect on the overall integral of the data and therefore the Zn/ H_2 stoichiometry does not change.

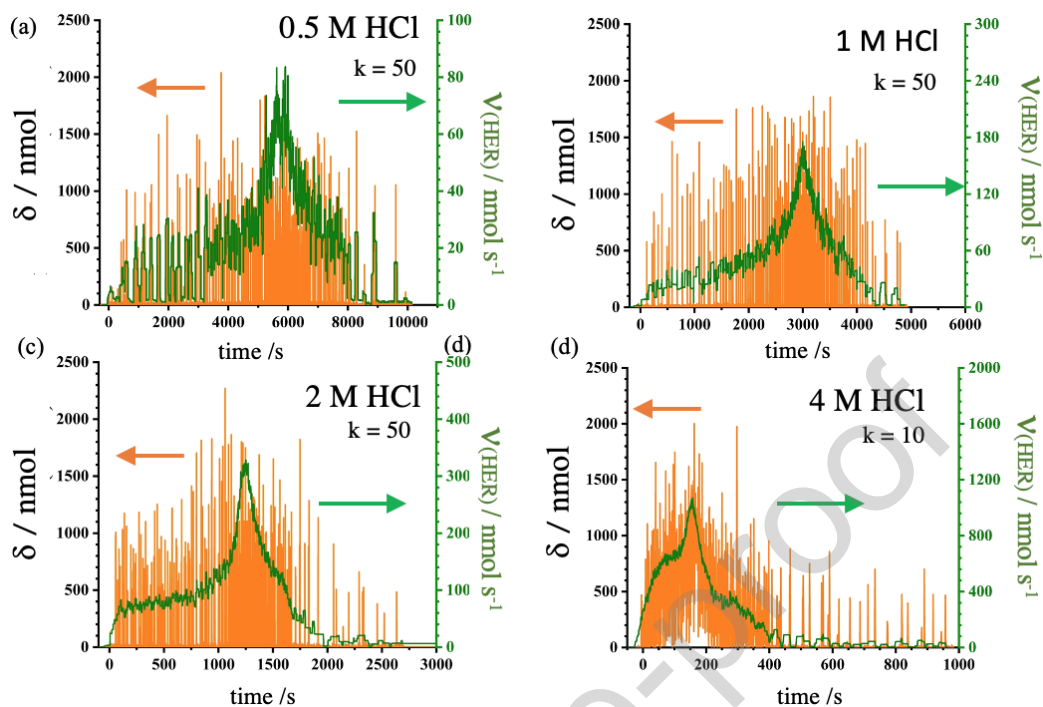


Fig. 7. Derivative of the quantity of H_2 , δ ($Q(H_2)$), from Fig. 4 using Eq. [7]. The ‘running’ average of 100 or 20 datapoints as a function of time using Eq. [8] is given in the second y-axis.

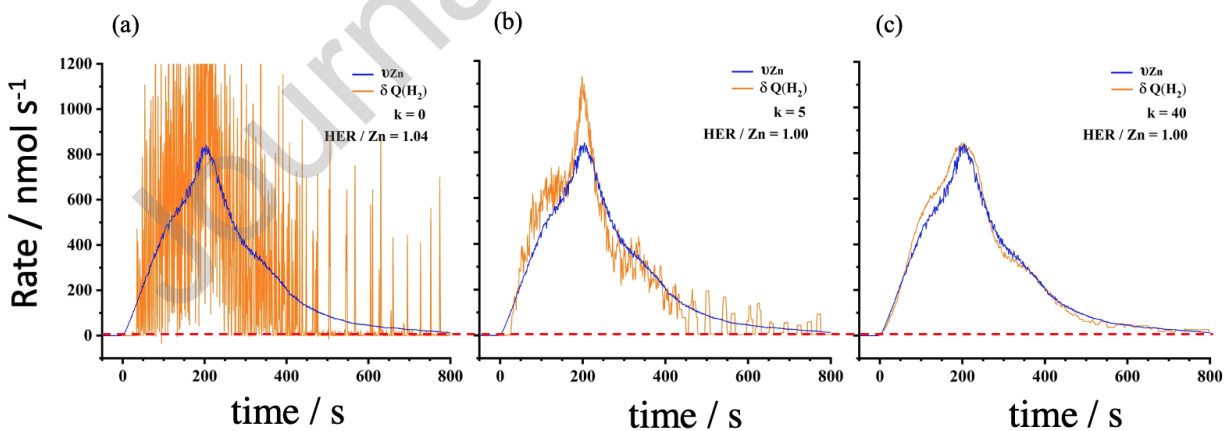


Fig. 8. The effect of smoothing on the raw gravimetric H_2 data from Fig. 7(d) in 4 M HCl. The Zn dissolution rate (v_{Zn}) is shown in blue. The HER rate data ($\delta Q(H_2)$) is shown in brown: a) no smoothing; b) smoothing $k = 5$; c) smoothing $k = 40$.

3.4 Mechanistic considerations

The correlation of elemental dissolution rates and the open circuit potential offers insights into the different stages of the spontaneous reaction of a galvanized steel coating with an acid solution. This is illustrated in Fig. 9 where the four stages of dissolution are indicated evidenced by changes in E_{oc} and the rates of elemental dissolution: (I) dissolution of Zn and Al when the intact Zn-Al alloy reacts with the electrolyte, (II) accelerated dissolution of Zn and Al when the Fe substrate is exposed due to bimetallic coupling, (III) dissolution of the Fe_2Al_5 intermetallic layer after removal of the Zn-Al coating, and finally (IV) dissolution of the steel substrate. This type of analysis is important for a deeper understanding of the different reaction steps during spontaneous open circuit reactions such as surface pickling and conversion coating treatments.

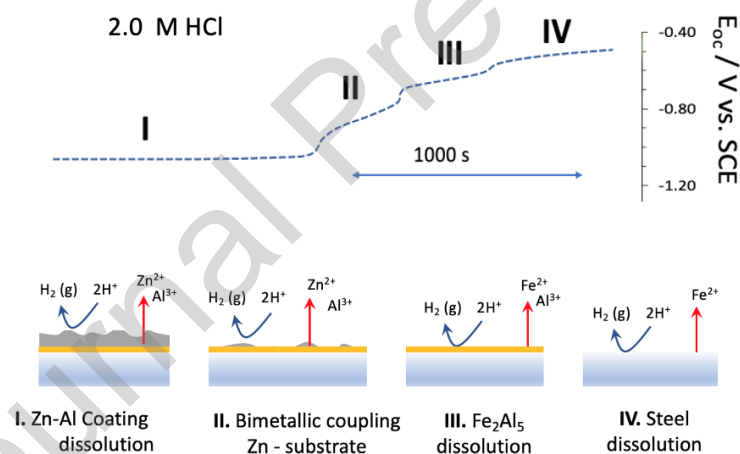


Fig. 9. Steps in the spontaneous reaction of a galvanized steel coating with HCl solution as determined by correlation of the open circuit potential with elemental dissolution rates.

4. Conclusions

In this work, a new approach to the simultaneous measurement of hydrogen evolution, alloy dissolution, and electrochemical potential and current was demonstrated. A linear correlation between the hydrogen evolution rate and applied cathodic current was observed for Pt in 1.0 M NaCl, for $-i_e \geq 5$ mA. At lower currents, the measured HER rate was systematically

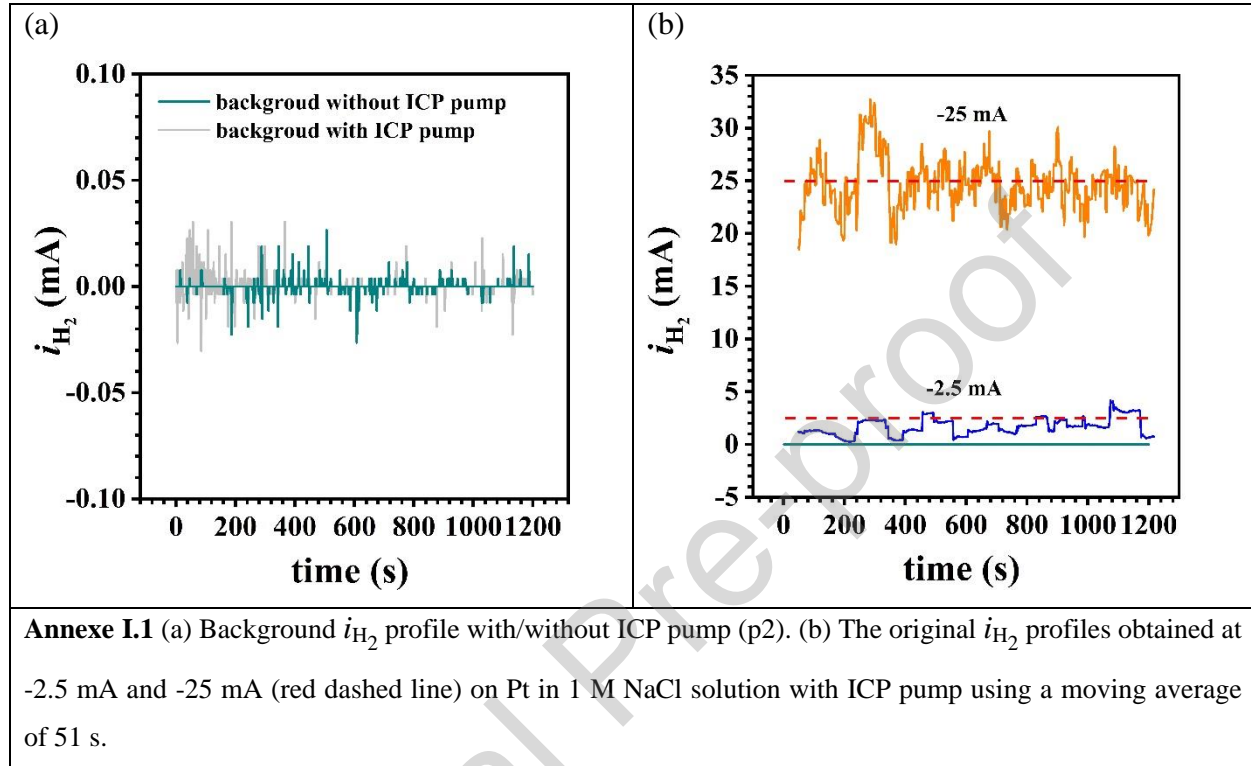
low perhaps due to the solubility of H_2 in the electrolyte. A validation experiment with a galvanized steel material is proposed and it is demonstrated that the measured Zn/ H_2 ratio is consistent with the expected 1:1 ratio. The total quantity with the 20 μm nominal thickness of the Zn coating was obtained consistent with the reported value. In addition to the relatively thick coating, it was demonstrated that the nanometric Fe_2Al_5 layer formed at the interface between the Zn coating and the steel, was quantifiable demonstrating the analytical capabilities of the AESEC technique. Four unique stages of dissolution were observed and indicated by changes in E_{oc} and the rates of elemental dissolution: (I) dissolution of Zn and Al when the intact Zn-Al alloy reacted with the electrolyte, (II) accelerated dissolution of Zn and Al when the Fe substrate was exposed due to bimetallic coupling, (III) dissolution of the Fe_2Al_5 intermetallic layer after removal of the Zn-Al coating, and finally (IV) dissolution of the steel substrate.

Acknowledgments

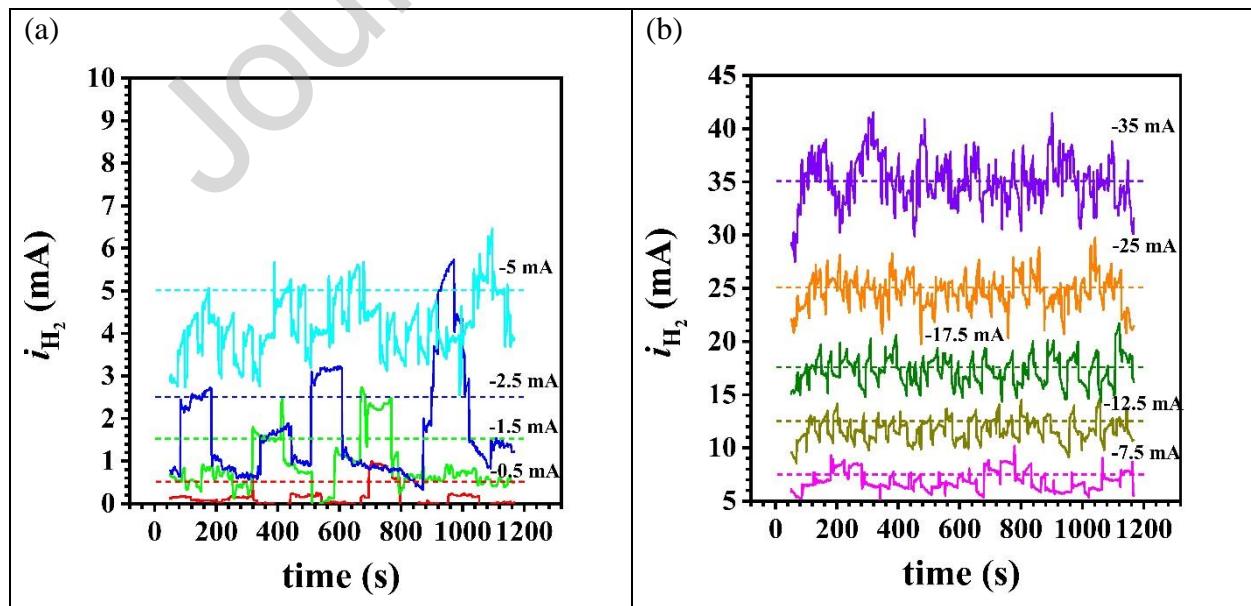
Author Baojie Dou expresses his gratitude to the China Scholarship Council (CSC) for financial support.

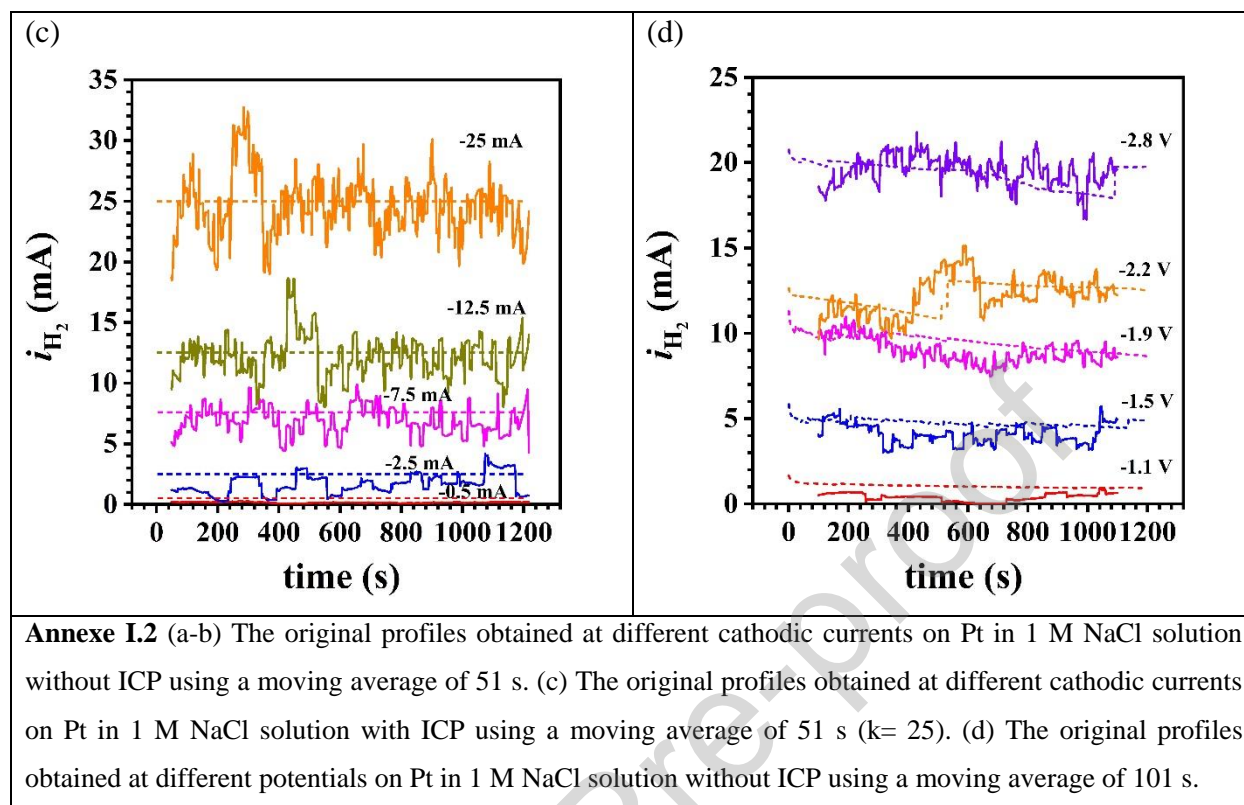
Annexe I

Annexe I.1



Annexe I.2





References

- [1] T.R. Thomaz, C.R. Weber, T. Pelegrini Jr., L.F.P. Dick, and G. Knörnschild, "The negative difference effect of magnesium and of the AZ91 alloy in chloride and stannate-containing solutions", *Corros. Sci.*, **52**(7), (2010) 2235-2243; <https://doi.org/10.1016/j.corsci.2010.03.010>.
- [2] G.S. Frankel, A. Samaniego, and N. Birbilis, "Evolution of hydrogen at dissolving magnesium surfaces", *Corros. Sci.*, **70**, (2013) 104-111; <https://doi.org/10.1016/j.corsci.2013.01.017>.
- [3] D. Eaves, G. Williams, and H.N. McMurray, "Inhibition of self-corrosion in magnesium by poisoning hydrogen recombination on iron impurities", *Electrochim. Acta*, **79**, (2012) 1-7; <https://doi.org/10.1016/j.electacta.2012.05.148>.
- [4] Z. Shi, and A. Atrens, "An innovative specimen configuration for the study of Mg corrosion", *Corros. Sci.*, **53**(1), (2011) 226-246; <https://doi.org/10.1016/j.corsci.2010.09.016>.
- [5] G. Song, A. Atrens, D.S. John, X. Wu, and J. Nairn, "The anodic dissolution of magnesium in chloride and sulphate solutions", *Corros. Sci.*, **39**(10-11), (1997) 1981-2004; [https://doi.org/10.1016/S0010-938X\(97\)00090-5](https://doi.org/10.1016/S0010-938X(97)00090-5).
- [6] J. Parascandola, and A. J. Ihde, "History of the Pneumatic Trough", *Isis*, **60**(3), (1969) 351-361; <https://doi.org/10.1086/350503>.
- [7] M. Curioni, "The behaviour of magnesium during free corrosion and potentiodynamic polarization investigated by real-time hydrogen measurement and optical imaging" *Electrochim. Acta*, **120**, 284-292 (2014); <http://dx.doi.org/10.1016/j.electacta.2013.12.109>.
- [8] M. Curioni, F. Scenini, T. Monetta, and F. Bellucci, "Correlation between electrochemical impedance measurements and corrosion rate of magnesium investigated by real-time hydrogen measurement and optical imaging", *Electrochim. Acta*, **166** (2015) 372-384; <https://doi.org/10.1016/j.electacta.2015.03.050>.
- [9] S. Fajardo, and G. S. Frankel, "Gravimetric method for hydrogen evolution measurements on dissolving magnesium", *J. Electrochem. Soc.*, **162** (2015) C693-C701; <https://doi.org/10.1149/2.0241514jes>.

-
- [10] C. Laurent, F. Scenini, T. Monetta, F. Bellucci, and M. Curioni, “The contribution of hydrogen evolution processes during corrosion of aluminium and aluminium alloys investigated by potentiodynamic polarisation coupled with real-time hydrogen measurement”, *npj Mat. Deg.* **1**, (2017) 1-7; <https://doi.org/10.1038/s41529-017-0011-4>.
- [11] J. M. Torrescano-Alvarez, M. Curioni, and P. Skeldon, “Gravimetric measurement of oxygen evolution during anodizing of aluminum alloys”, *J. Electrochem. Soc.*, **164**(13), (2017) C728-C734; <https://doi.org/10.1149/2.0371713jes>.
- [12] M. G. Strelb, M. Bruns, and S. Virtanen, “Editors' Choice—Respirometric in situ methods for real-time monitoring of corrosion rates: Part I. Atmospheric corrosion”, *J. Electrochem. Soc.*, **167**(2), (2020) 021510 ; <https://doi.org/10.1149/1945-7111/ab6c61>.
- [13] S. Lebouil, A. Duboin, F. Monti, P. Tabelaing, P. Volovitch, and K. Ogle, “A novel approach to on-line measurement of gas evolution kinetics: Application to the negative difference effect of Mg in chloride solution”, *Electrochim. Acta*, **124**, (2014) 176-182 ; <http://dx.doi.org/10.1016/j.electacta.2013.07.131>.
- [14] S. Lebouil, O. Gharbi, P. Volovitch, and K. Ogle, “Mg dissolution in phosphate and chloride electrolytes: insight into the mechanism of the negative difference effect”, *Corrosion*, **71**(2), (2015) 234-241; <http://doi.org/10.5006/1459>.
- [15] J. Han, and K. Ogle, “Communication—Hydrogen evolution and elemental dissolution by combined gravimetric method and atomic emission spectroelectrochemistry”, *J. Electrochem. Soc.*, **166**(11), (2019) C3068-C3070; <https://doi.org/10.1149/2.0091911jes>.
- [16] D. Zapico-Álvarez, F. Bertrand, J. -M. Mataire, and M.-L. Giorgi, “Nature of the inhibition layer in GA baths”, *Metall. Res. Technol.*, **111**, (2014) 9–15; <https://doi.org/10.1051/metal/2014002>.
- [17] D. Zapico-Álvarez, P. Barges, C. Musik, F. Bertrand, J. -M. Mataire, M. Descoins, D. Mangelinck, and M.-L. Giorgi, “Further Insight into Interfacial Interactions in Iron/Liquid Zn-Al System”, *Metall. Mater. Trans. A*, **51**, (2020) 2391-2403; <https://doi.org/10.1007/s11661-020-05669-5>.
- [18] E. Baril, and G. L'Espérance, “Studies of the morphology of the Al-rich interfacial layer formed during the hot dip galvanizing of steel sheet”, *Metal. Mat. Trans. A*, **30**, (1999) 681–695; <https://doi.org/10.1007/s11661-999-1000-1>.
- [19] A. R. Marder, “The metallurgy of zinc-coated steel”, *Prog. Mater. Sci.*, **45**(3), (2000) 191-271; [https://doi.org/10.1016/S0079-6425\(98\)00006-1](https://doi.org/10.1016/S0079-6425(98)00006-1).
- [20] M. Guttmann, “Diffusive phase transformations in hot dip galvanizing”, *Mater. Sci. Forum*, **155–156**, (1994) 527-548; <https://doi.org/10.4028/www.scientific.net/MSF.155-156.527>.
- [21] K. Ogle, P Lodi, and A. Storhay, “Method of analysis of a metallic sample by dissolving the surface thereof and device for carrying out said method”, WO Patent WO/1993/019,365; (<https://patents.google.com/patent/WO1993019365A1/en>).
- [22] K. Ogle, “Atomic emission spectroelectrochemistry: Real-time rate measurements of dissolution, corrosion, and passivation”, *Corrosion*, **75**(12), (2019) 1398-1419; <https://doi.org/10.5006/3336>.
- [23] Bulletin météo de la station PARIS-MONTSOURIS, (<https://www.ventusky.com/paris>)
- [24] https://materials.springer.com/isp/crystallographic/docs/sd_1201135, retrieved March 28th, 2022.
- [25] O. Gharbi, N. Birbilis, and K. Ogle, “In-situ monitoring of alloy dissolution and residual film formation during the pretreatment of Al-alloy AA2024-T3”, *J. Electrochem. Soc.*, **163**(5), (2016) C240-C251; <https://doi.org/10.1149/2.1121605jes>.
- [26] K. Ogle, and S. Weber, “Anodic dissolution of 304 stainless steel using atomic emission spectroelectrochemistry”, *J. Electrochem. Soc.*, **147**(5), 1770-1780 (2000). <https://doi.org/10.1149/1.1393433>
- [27] V. Shkirskiy, P. Maciel, J. Deconinck, and K. Ogle, “On the time resolution of the atomic emission spectroelectrochemistry Method”, *J. Electrochem. Soc.* **163**(201) C37, <https://doi.org/10.1149/2.0991602jes>

Table Captions

Table 1. Integration of each alloying elements and corrected H_2 in μmol from Fig. 4. Al and Fe were calculated from the third domain (III) to investigate the stoichiometry of the intermetallic phase.

Figure Captions

Fig. 1.

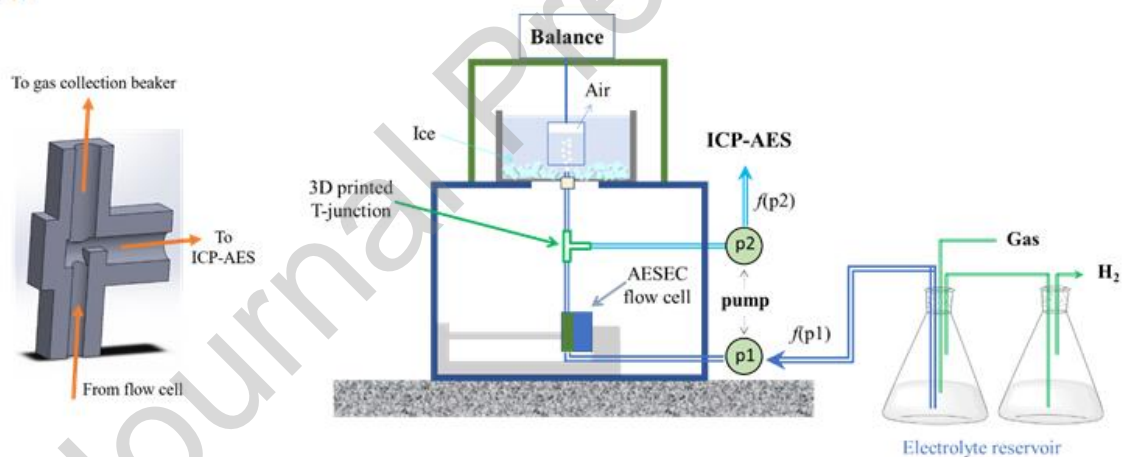


Fig. 1. Schematic of the experimental set-up. The 3D printed T-junction is shown to the left.

Fig. 2.

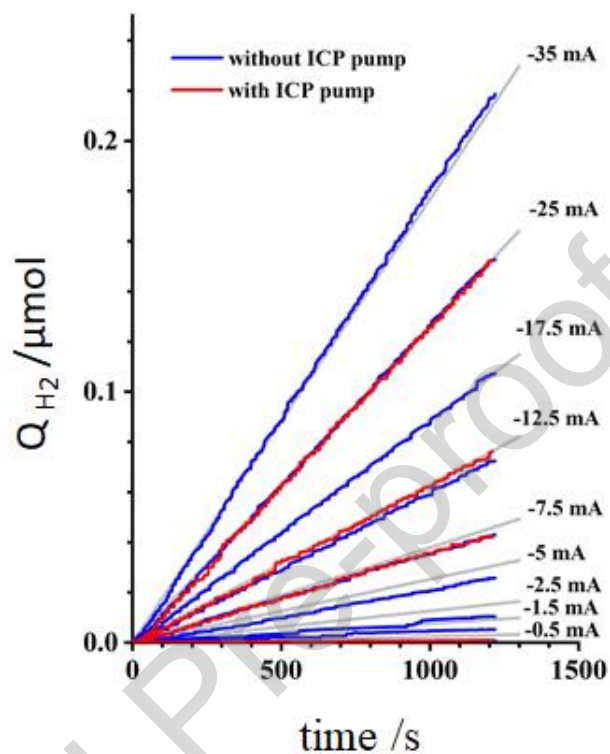


Fig. 2. Quantity of H_2 determined from the recorded mass change (Eqs. [5] and [6]) as a function of time for Pt in 1.0 M NaCl, pH = 6.4 as indicated. The gray lines represent the expected values for the applied current assuming Faraday's law with 100% cathodic efficiency. The electrode surface area was 0.5 cm^2 . Red and blue curves were recorded with and without the ICP-AES pump (p2 in Fig. 1).

Fig. 3.

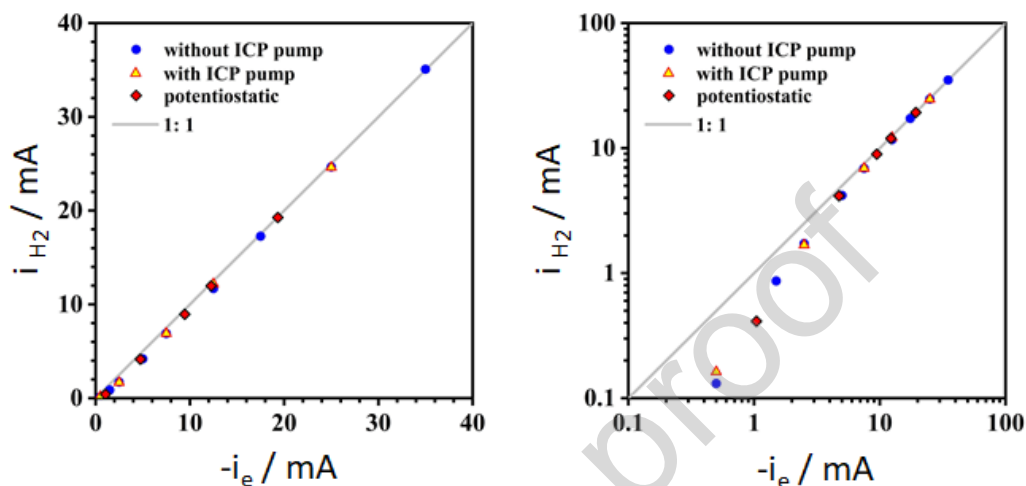


Fig. 3. Quantity of H_2 as a function of the applied cathodic current ($-i_e$). The electrode surface area was 0.5 cm^2 . The red diamonds are the results of potentiostatic experiments in which the HER rate is plotted versus the average of the cathodic current density ($-i_e$) transient. The log-log plot (right) is shown to better illustrate the difference in the low current range, $-i_e < 5 \text{ mA}$. The solid line indicates the hypothetical 1:1 relationship. The original profiles are available in **Annexe I.2**.

Fig. 4.

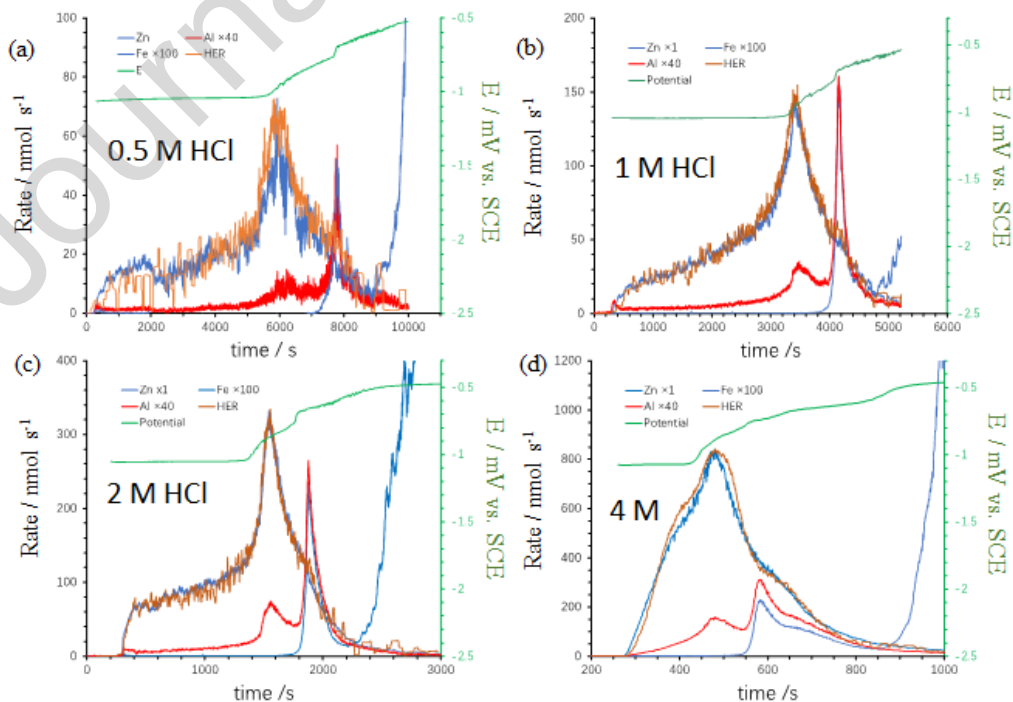


Fig. 4a.

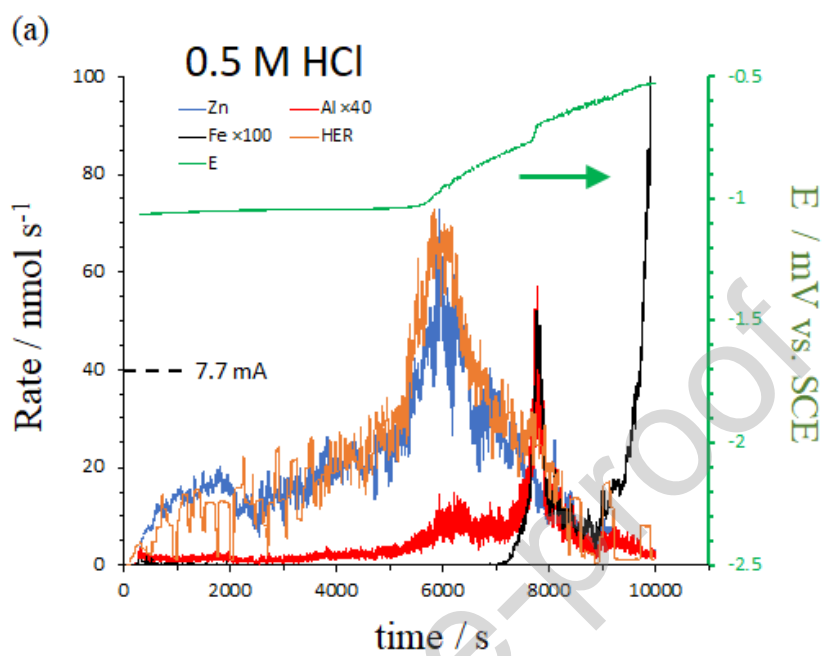


Fig. 4b.

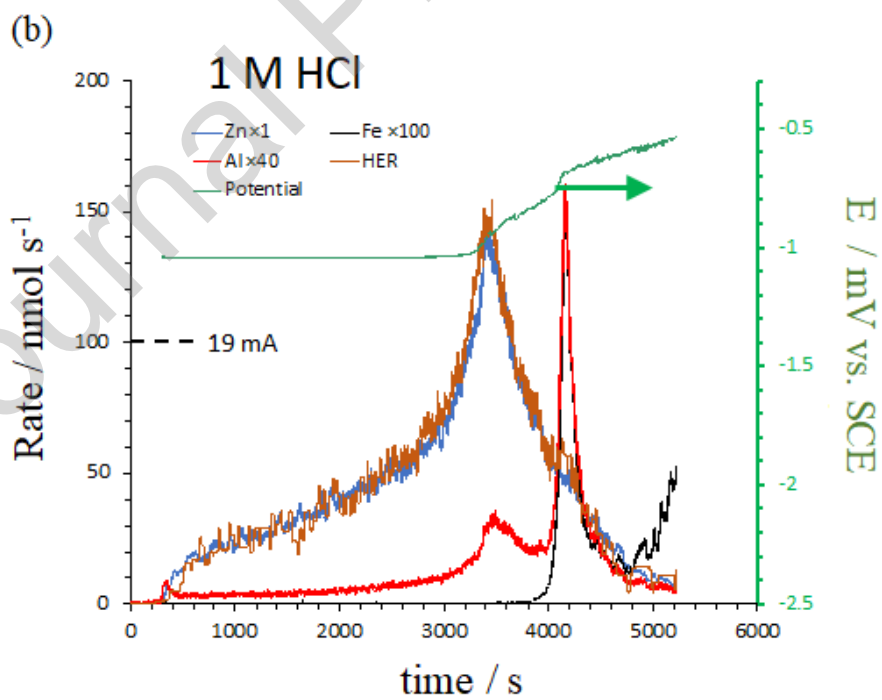


Fig. 4c.

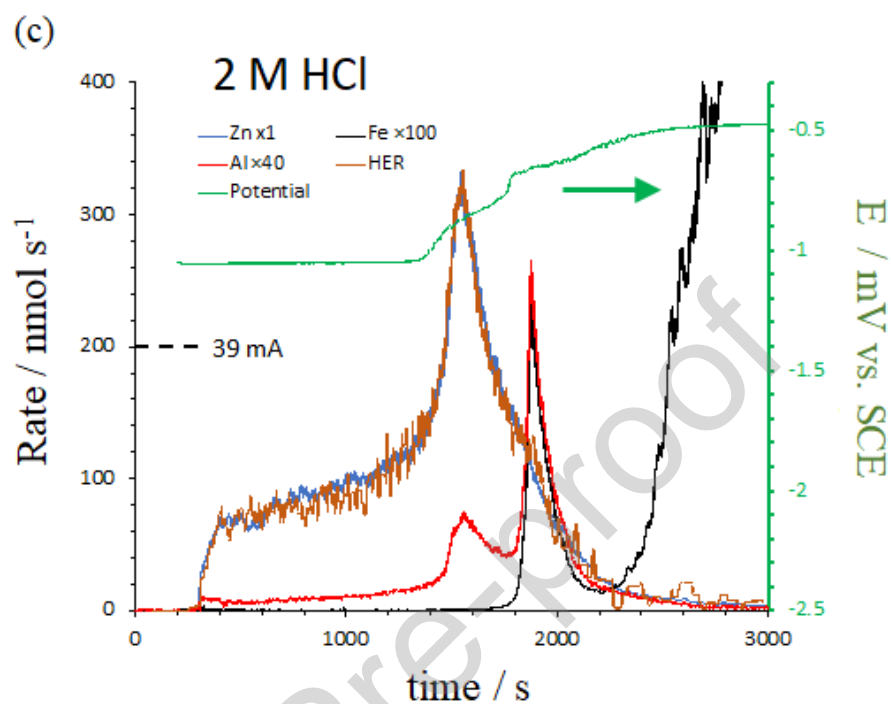


Fig. 4d.

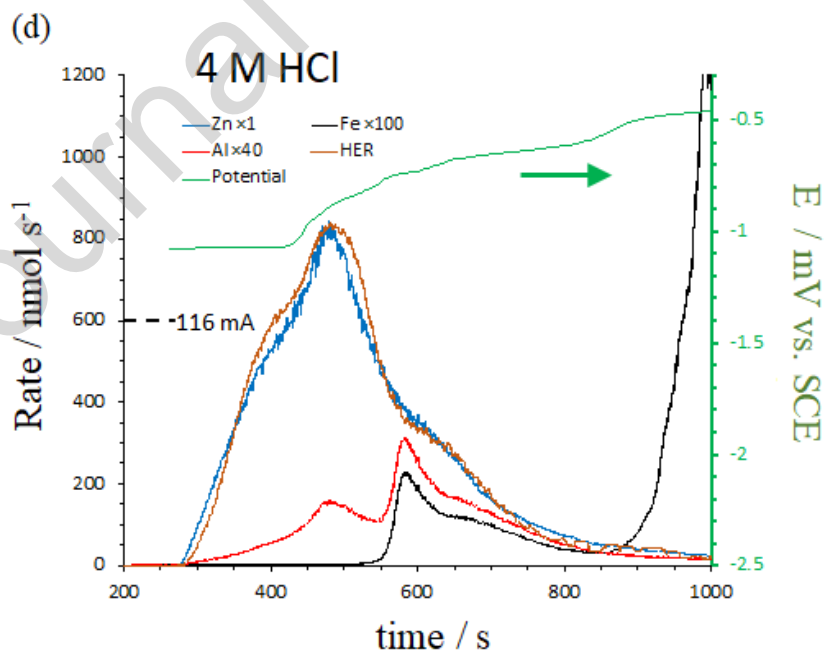


Fig. 4. Open circuit dissolution profiles of a Zn-Al galvanized steel coating in HCl with different concentrations showing Zn, Al, and Fe elemental dissolution rates, HER rates, and the open circuit potential

(E) as a function of time. The surface area was 1.0 cm^2 . The current values provided on the y-axis indicate equivalent currents corresponding the elemental dissolution rates for comparison with Fig. 3.

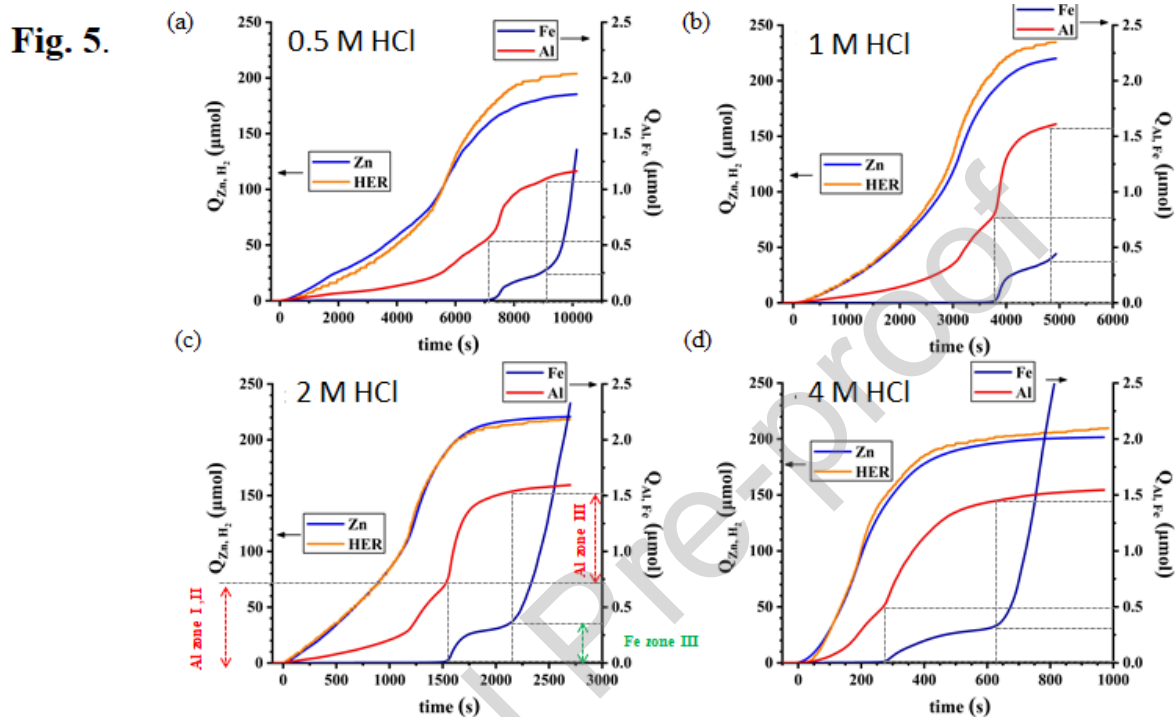


Fig. 5a.

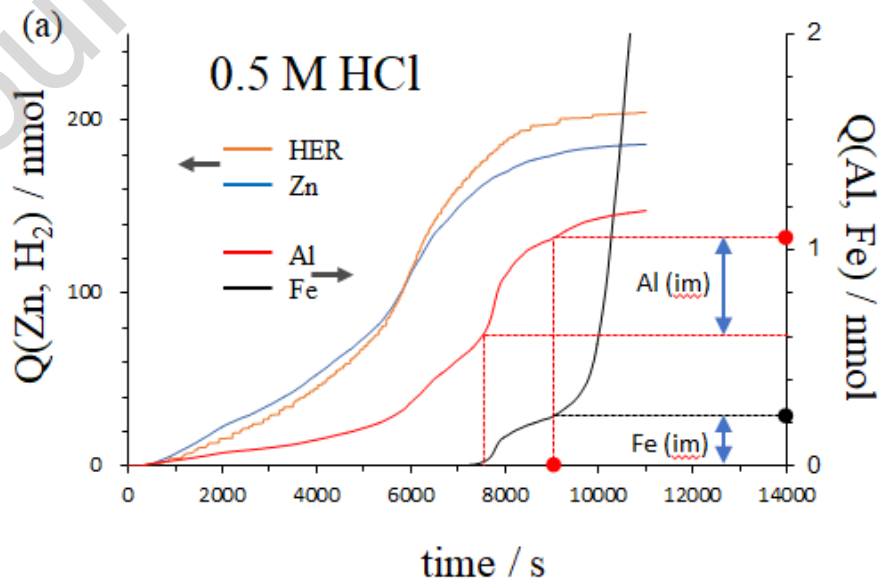


Fig. 5b.

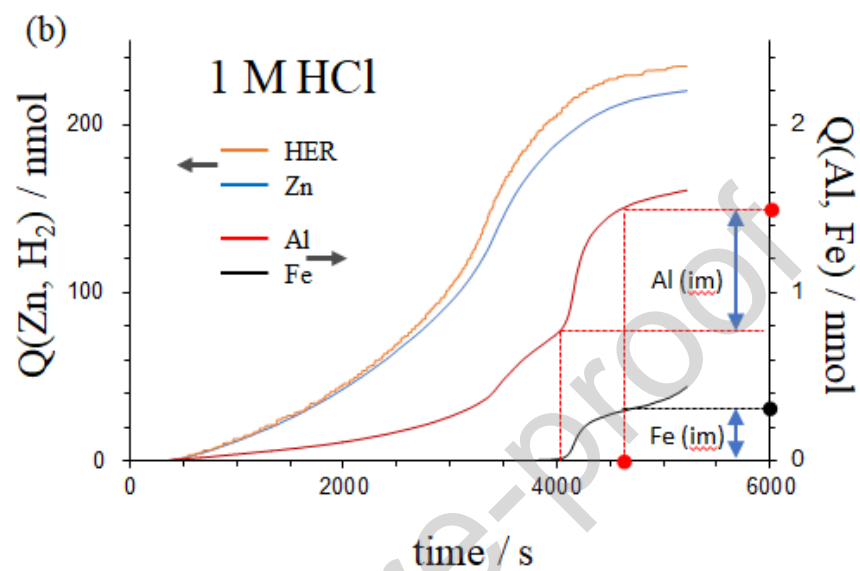


Fig. 5c.

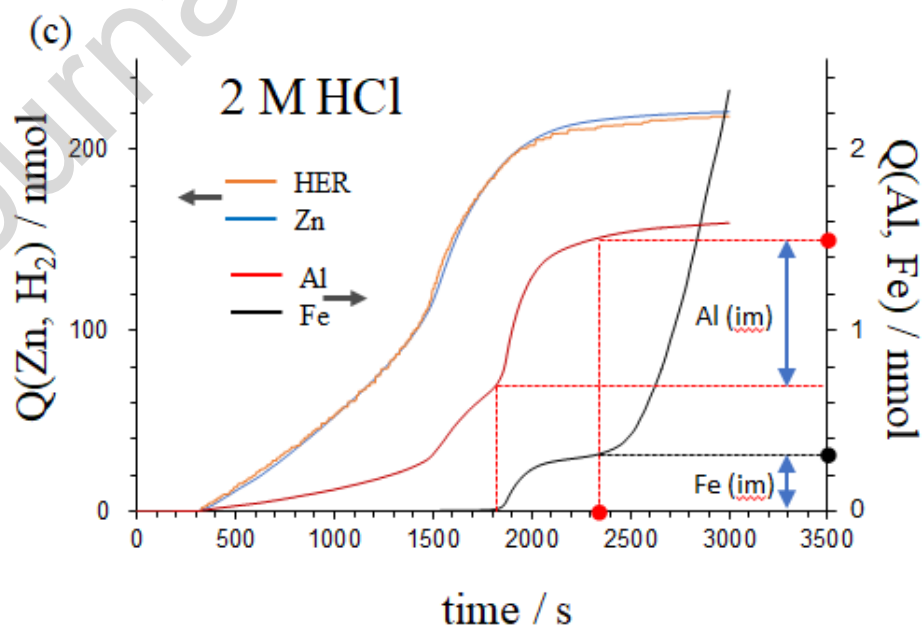


Fig. 5d.

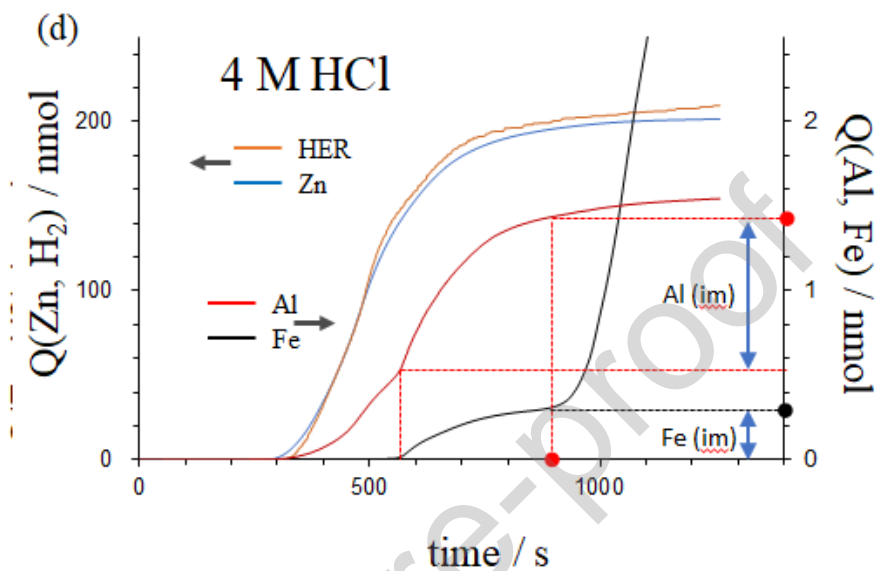


Fig. 5. Quantity of each alloying element and HER integrated from dissolution profiles of Fig. 4. The dashed lines show the method of determining the quantity of Al and Fe in the interfacial Al-Fe alloy (zone III).

Fig. 6.

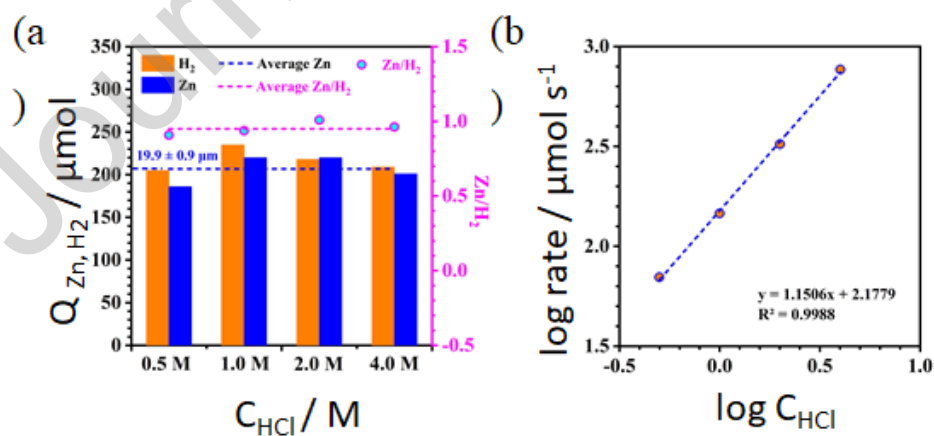


Fig. 6. (a) Quantitative analysis of Zn and H₂ as a function of HCl concentration revealing an estimated coating thickness of a 20 ± 1 μm Zn-Al galvanized coating. (b) The maximum dissolution rate of Zn (or the

HER rate assuming they are 1:1) vs. HCl concentration (from Fig. 4), revealing a first order reaction rate dependence.

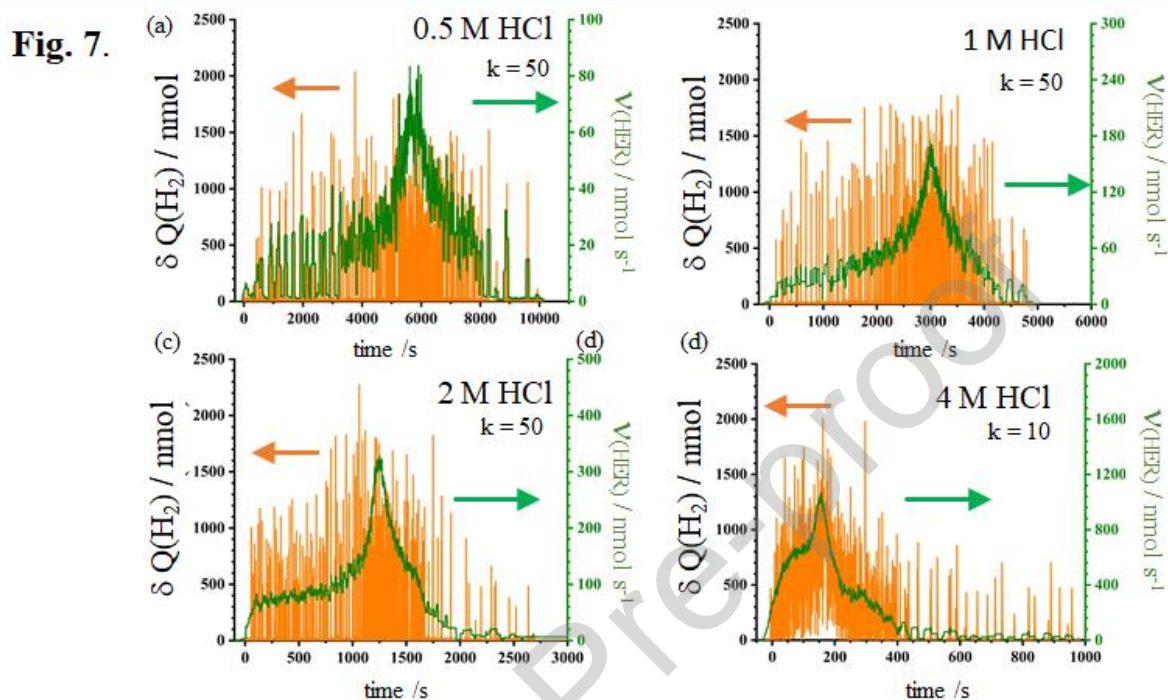


Fig. 7. Derivative of the quantity of H_2 , $\delta(Q(H_2))$, from Fig. 4 using Eq. [7]. The ‘running’ average of 100 or 20 datapoints as a function of time using Eq. [8] is given in the second y-axis.

Fig. 8

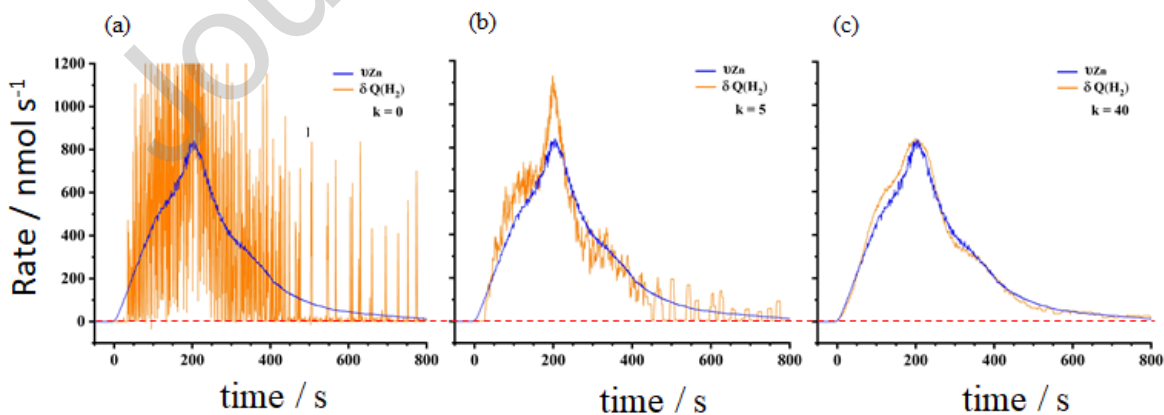


Fig. 8. The effect of smoothing on the raw gravimetric H_2 data from Fig. 7(d) in 4 M HCl. The Zn dissolution rate (v_{Zn}) is shown in blue. The HER rate data ($\delta Q(H_2)$) is shown in brown: a) no smoothing; b) smoothing $k = 5$; c) smoothing $k = 40$.

Fig. 9.

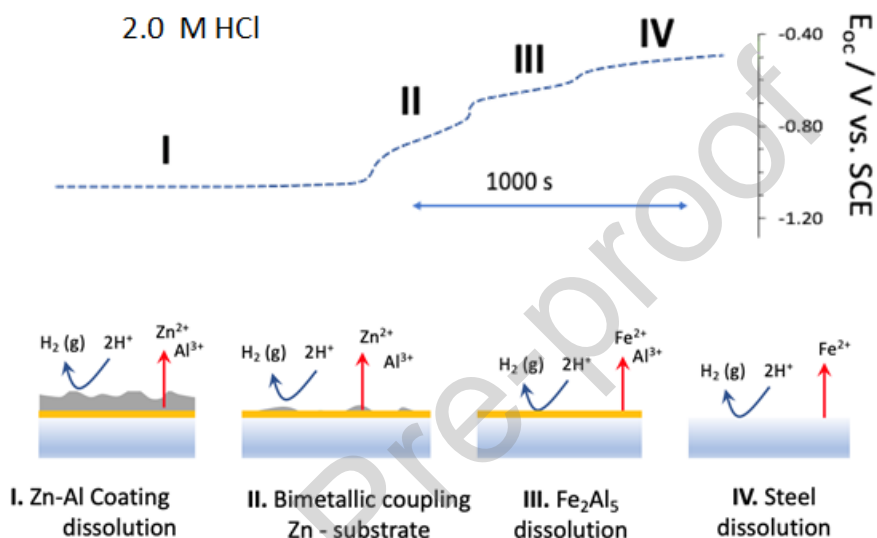
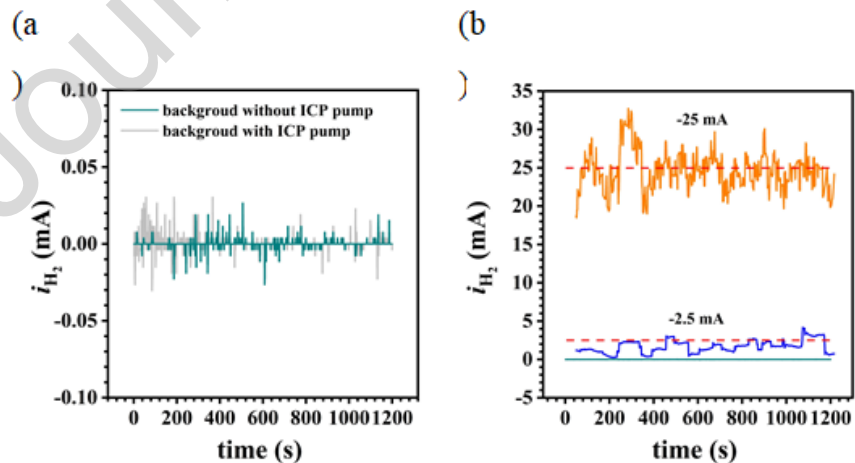


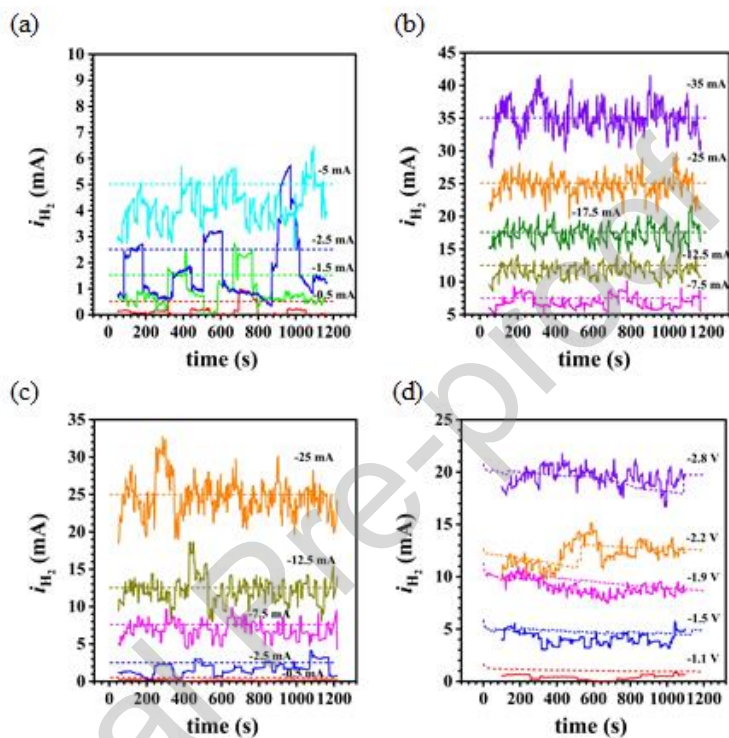
Fig. 9. Steps in the spontaneous reaction of a galvanized steel coating with HCl solution as determined by correlation of the open circuit potential with elemental dissolution rates.

Annexe I.1



Annexe I.1 (a) Background i_{H_2} profile with/without ICP pump (p2). (b) The original i_{H_2} profiles obtained at -2.5 mA and -25 mA (red dashed line) on Pt in 1 M NaCl solution with ICP pump using a moving average of 51 s.

Annexe I.2



Annexe I.2 (a-b) The original profiles obtained at different cathodic currents on Pt in 1 M NaCl solution without ICP using a moving average of 51 s. (c) The original profiles obtained at different cathodic currents on Pt in 1 M NaCl solution with ICP using a moving average of 51 s ($k=25$). (d) The original profiles obtained at different potentials on Pt in 1 M NaCl solution without ICP using a moving average of 101 s.

CRedit authorship contribution statement

B. D., X. L. and J. H. designed the experimental apparatus and conducted the experiments. B.D. wrote the first manuscript. K. O. conceived the experimental plan and supervised the experiments.

Declaration of interests

The authors declare that they have no known competing financial interests or personal relationships that could have appeared to influence the work reported in this paper.

The authors declare the following financial interests/personal relationships which may be considered as potential competing interests:

Highlights

- A novel AESEC-Gravimetric system was invented to monitor the element dissolution rate, gas formation, and electrical current simultaneously.
- The different stages of galvanized steel dissolution (coating, interfacial alloy, steel substrate) were resolved in the dissolution profile.
- The Zn/H₂ ratio is equal to an expected 1:1 was verified by the spontaneous reaction of galvanized steel in HCl solution.
- The nanometric Fe₂Al₅ layer between the Zn coating and the steel was quantifiable demonstrating the analytical capabilities of the AESEC system.